Open Access Research Journal of
Life Sciences
Journals home page: https://oarjpublication/journals/oarjls/
ISSN: 2783-025X (Online)

OARJ OPEN ACCESS RESEARCH JOURNALS

(RESEARCH ARTICLE)

Check for updates

A quantitative histological study of the expression of Snail and Cytokeratin 18 in benign prostatic hyperplasia and prostatic adenocarcinoma

Luis Santamaría [1,*], Ildefonso Ingelmo [2] and Fernando Teba [3]

[1] *Department of Anatomy, Histology, and Neuroscience. School of Medicine, Autonomous University of Madrid, Madrid, Spain.*
[2] *Department of Anesthesiology. Hospital Ramón y Cajal, Madrid, Spain.*
[3] *Department of Surgery (Urology), Hospital de La Princesa, School of Medicine, Autonomous University of Madrid, Spain.*

Open Access Research Journal of Life Sciences, 2022, 04(02), 050–062

Publication history: Received on 26 October 2022; revised on 03 December 2022; accepted on 05 December 2022

Article DOI: https://doi.org/10.53022/oarjls.2022.4.2.0078

Abstract

The purpose of this study is to quantify from a histological point of view, the expression of Snail, both nuclear and cytoplasmic, correlating it with cytokeratin 18 immunoreactivity in normal prostate, benign prostate hyperplasia, and prostate cancer by estimates of integrated optical density per unit area in arbitrary units of uncalibrated optical density per μm^2. These estimates will be made both globally and locally to verify the heterogeneity of these markers. Linear regression was applied to investigate the correlation between the expression of Snail and the expression of cytokeratin 18 in the study groups. Discriminant analysis performed to classify the cases in the study groups was also applied using Snail and cytokeratin 18 measurements as classifying variables. In all cases, Snail's immunoexpression is heterogeneous with local variations. In cancer, the expression of Snail is abundant at the nuclei, while in normal and hyperplastic tissue Snail is mainly cytoplasmic, which may indicate that in these situations, Snail predominates in an inactive form. The expression of Snail is negatively correlated with that of the epithelial marker cytokeratin 18; this could be correlated with mesenchymal epithelium transition developed in the cancer progression. Snail and cytokeratin 18 immunoexpression were able to discriminate between normal, hyperplastic, and malignant prostate tissues.

Keywords: Prostate cancer; Benign Prostatic Hyperplasia; Snail; Cytokeratin 18; Epithelial-mesenchymal transition

1. Introduction

The histological changes detected in prostate pathology, both benign and malignant, show great local variability. Benign prostatic hyperplasia (BPH) is heterogeneous in tissue morphometry and expression of single essential genes [1]. Regarding malignant lesions, prostate cancer is a tumor that is usually made up of a multitude of cell lines that interact with each other and with non-tumor tissue, causing frequent intratumoral heterogeneity that explains the great variability that these cancers show in terms of recurrence and their invasiveness local and its dissemination at a distance [2, 3].

The epithelial cells can undergo epithelial-mesenchymal transition (EMT) during prostate cancer progression, manifested by structural changes in their phenotype from columnar cells to spindle-shaped. This is associated with down-regulation of some epithelial cell markers such as E-cadherin and occludins, which leads to loss of intercellular adhesion, while mesenchymal markers such as vimentin and N-cadherin are up-regulated, allowing cells to move and migrate to other organs [4, 5]; also, the expression of these markers was correlated with an increase in cell proliferation [6].

* Corresponding author: Luis Santamaría
Department of Anatomy, Histology, and Neuroscience. School of Medicine, Autonomous University of Madrid, Madrid, Spain.

Interestingly, EMT also plays a role in the development and evolution of benign conditions such as BPH. Until recently, EMT has only been linked to the onset of BPH, however, there are morphological data that suggest that the increase of phenotypically mesenchymal cells derived from the prostate epithelium is related to the development of BPH [7, 8]. Some studies have observed areas of the ductal epithelium where cells do not express E-cadherin, lose their functional polarity, and become spindle-shaped. All this leads to the conclusion that in BPH there is no actual mesenchymal proliferation, but rather an accumulation of mesenchymal cells derived from the prostate epithelium [9].

Furthermore, EMT markers have been detected, both in BPH and in prostate cancer, for example mesenchymal markers such as N-cadherin, vimentin and fibronectin. Likewise, several transcription factors have been observed, among them Snail that act as repressors of E-cadherin. Subsequently, a decrease in markers of epithelial origin such as E-cadherin, B-catenin, cytokeratins and desmoplakin is detected in EMT [5, 10, 11].

In this study, we will focus on possible local changes in the expression of Snail, both in BPH and cancer. Snail was first described in Drosophila melanogaster [12-14], where it was shown to be essential for the formation of the mesoderm [15]. Besides, Snail homologues have been found in many species, including humans. Snail and its homologues have a role in promoting cell displacement, including phenomena such EMT where Snail was shown to transform epithelial cells into mesenchymal cells through the direct repression of E-cadherin expression [16, 17]. As indicated above, Snail downregulates several epithelial markers, such as desmoplakin, the epithelial mucin Muc-1, and cytokeratin-18 [13].

The purpose of this study is to quantify, from a histological point of view, the expression of Snail, both nuclear and cytoplasmic, correlating it with immunoreactivity for cytokeratin-18 (ck18) in normal prostate, benign prostate hyperplasia, and in prostate cancer. These estimates will be made both globally and locally to verify the possible heterogeneity of these markers.

2. Material and methods

Thirty prostate specimens were collected from La Princesa Hospital (Madrid, Spain), ten were from adults, (CTR), age (mean±SD): 45±7; range: 30-47 years, all these specimens were of healthy subjects, without endocrine or reproductive pathology, deceased in traffic accidents, and eligible as donors for transplant, ten were surgical specimens (adenomectomies) from patients diagnosed of the adenofibromiomatous type of benign prostatic hyperplasia, (BPH), age (mean ± SD): 75 ± 10, range: 65-85 years, the other ten were surgical specimens (radical prostatectomy) from patients diagnosed with prostate carcinoma (CA): age (mean±SD): 70±10, range: 56 to 85 years. The diagnosis was confirmed by histopathology. Cancer cases were graded according to Gleason's score [18, 19]; only cases with a grade of 7(3 + 4) or 7(4 + 3) were included in the study. All cases were without prior neoadjuvant hormonal therapy. Ethical requirements were accomplished to obtain the prostatic tissue during the multi-organic extraction for transplant (CTR) or at the surgery (BPH and CA).

2.1. Processing of the tissues

The specimens were fixed for a week in 10% paraformaldehyde in PBS, pH 7.4. After fixation, each specimen from the three groups was thoroughly sectioned into 2-mm-thick slices, performed by isotropic uniform random sampling (IUR sections) [20] to preserve the isotropy of the tissue to implement all stereological estimates. All the slices were processed for paraffin embedding. Thirty sections (5-µm-thick) were performed on each block for immunohistochemistry.

2.2. Immunohistochemistry

At least 10 randomly selected slides per specimen were immunostained in CTR, BPH, and CA groups to detect Snail and ck18 immunoreactivities. Sections were incubated either with a rabbit polyclonal antibody to Snail (Abcam, Cambridge, UK) or with a monoclonal anti-cytokeratin-18 antibody (Abcam, Cambridge, UK), both diluted at 1:250.

Pretreatment of sections by heat [21] was performed to enhance Snail and ck18 immunostaining. Other studies have widely described the rationals for immunohistochemistry [22-24].

2.3. Data acquisition

Three strips of ten immediately adjacent quadrats were explored for both Snail and ck18 immunostained sections from CTR, BPH, and CA groups. The origin and sense of the axis for each strip were chosen by systematic random sampling [25] for all the strips. The result was a series of images from the three groups, sized 512 × 6800 pixels. The final magnification (x1000) for Snail strips was such that 6800 pixels represented 855 µm. At that point, the strips were 8.5 mm long. Therefore, the total length explored per section (ten sections) and per case (at least 10 cases) was 8.5 × 10 × 10 = 850 mm (for CA cases, an appreciable percentage of the maximum specimen diameter) [26]. Likewise, the final

magnification (x100) for the study of the immunostained strips for ck18 was such that 6800 pixels represented 8550 µm. Thus, the total length of the ck18 strip was the same as that explored for the immunostaining for Snail.

The images were captured using a color digital camera DP 70 (Olympus Corporation of the Americas, PA, USA) with a resolution of 12.5 megapixels, attached to an Olympus microscope fitted with a motorized stage controlled by the stereological software Cast-Grid (Stereology Software Package, Silkeborg, Denmark). This program monitors the XY displacement of the microscope stage. It allows the selection of fields to be studied by systematic random sampling after inputting an appropriate sampling fraction [3].

The strips were then mounted from the images captured, using the public domain Java image processing program, Image J (version 1.48), developed at the US National Institutes of Health and available at https://imagej.nih.gov/ij/index.html [27]. Subsequently, the resultant strips were processed using the same software. As indicated below, different protocols were followed to process the immunostained strips for Snail and ck18 to estimate the parameters under study.

- Quantification of immunoreactivity for Snail expressed in prostate epithelial nuclei: In all study groups, the strips made on the preparations immunostained for Snail (Figure 1a), were processed to segment the immunostained epithelial nuclei (Figure 1b), using a plugin integrated in the Image J software. The strips thus modified were stored for later quantification.
- Quantification of immunoreactivity for Snail expressed in the cytoplasm of prostate epithelium: A subtraction operator was employed using the Image J software to exclude the immunostained nuclei from the original strips, obtaining new strips with only the cytoplasmic immunostaining for Snail (Figure 1c), which were also stored to quantify the Snail immunoreactivity of the prostate epithelial cytoplasm.
- Quantification of immunoreactivity for ck18 expressed in the cytoplasm of prostate epithelium: In all study groups, the strips made on the preparations immunostained for ck18, were processed to segment the immunostained epithelial cytoplasms (Figure 1d), using a plugin integrated in the Image J software. The strips thus processed were stored for later quantification.

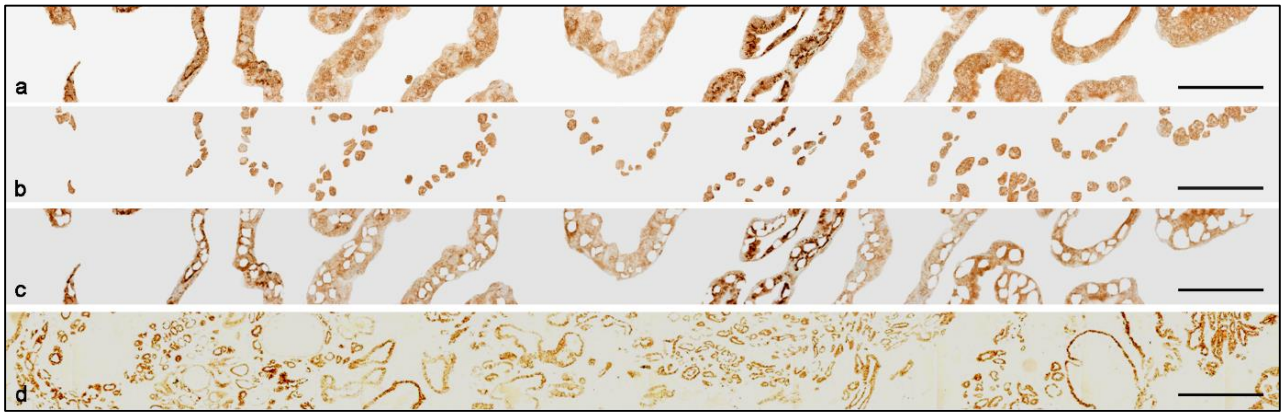

Figure 1 In (a) the image shown is a strip from a specimen of CA group immunostained to Snail; in (b) the image from (a) was processed to segment the immunostained epithelial nuclei; the image from (c) represents the result of substraction from (a) minus (b) resulting the visualization of Snail immunoreactive cytoplams. In (d), the image shown is a strip from a specimen of CA group immunostained to ck18. The scale bars from (a-c) represent 57 µm, and the scale bar from (d) represents 570 µm

2.4. Quantitative methods for Snail and ck18 immunostainings

There are abundant references on the use of integrated optical density for quantification in immunohistochemistry [28-30], specifically concerning immunostaining carried out on prostate tissue [31-33]. Therefore, in the present study, local and global estimates of integrated optical density will be used at the nuclear and cytoplasmic levels to estimate the immunoexpression of the antibodies used.

Local measurements of integrated optical density per unit area expressed in arbitrary units of uncalibrated optical density per μm^2 (IOD) were obtained, both for nuclear and cytoplasmic immunostaining for Snail and cytoplasmic immunostaining for ck18.

Each strip was segmented into orthogonal columns whose height was equal to the height of the entire strip, and the width was set at 19 µm for Snail strips, and at 190 µm for ck18 strips; so that the entires Snail strips were subdivided into a total of 45 columns (19 x 45 = 855 µm), and the ck18 strips also were subdivided into a total of 45 columns (190

x 45 = 8550 μm). IOD was automatically recorded by the image analysis system for all the columns orthogonal to the long axis. The resulting series of 45 consecutive rational numbers per visual field served as input signals for estimating the IOD measurements (per μm^2 of either nuclear or cytoplasmic area) [26]. Results were plotted as a space series, being position in μm represented in the X-axis and the IOD in the Y-axis of the plot.

The global measurement of IOD for Snail immunostaining was obtained, averaging the local IOD over the total number of strips for each case in CTR, BPH, and CA groups.

2.5. Statistical analysis

For IOD values along the space series, the local estimates of mean ± SEM for either Snail (nuclear and cytoplasmic) or ck18 (cytoplasmic) were performed and compared between CTR and BPH and between CTR and CA by a Student t-test. In addition, local estimates of IOD in CTR, BPH, and CA were compared intragroup.

The following comparisons were made using ANOVA between the three study groups (CTR, BPH, and CA): Global IOD of nuclear Snail; Global IOD of cytoplasmic Snail; Global IOD of ck18. The global IOD values in the three study groups, for Snail and ck18, were expressed as mean ± SEM. The Newman–Keuls test performed comparisons between the means for all the groups studied.

Linear regression was applied to investigate the possible correlation between the expression of Snail (nuclear or cytoplasmic) and the expression of ck18 in the study groups. On the one hand, the case populations subjected to linear regression were (CTR + BPH) and on the other (CTR + CA). The independent variable was ck18 IOD in all cases, while the dependent variables were either nuclear Snail IOD or cytoplasmic Snail IOD. For all the comparisons, the level of significance was $p < 0.05$.

To find out which were the variables that classify most accurately cases in the groups (CTR, BPH, and CA) considered, stepwise linear discriminant analysis was applied to the study groups for the different local variables: nuclear Snail IOD, cytoplasmic Snail IOD, and ck18 IOD. According to Wilks' lambda, the discriminant variables were selected at each step. The variable that minimizes the overall Wilks' Lambda or maximizes the associated F statistic (F to enter = 3.84 and F to remove = 2.71). Lambda Wilks's statistic explains the rate of total variability that is not due to differences among groups. A lambda of 1 means that the mean of the discriminant scores is the same in all groups, and there are no variability between groups, and a lambda near 0 means that there is a big difference among groups. Therefore, Wilk's lambda provides a test of the null hypothesis that the population means are equal. The larger lambda is, the less discriminating power is present [34]. The variables included in the analysis could define discriminant functions, whose graphic representation will show the clustering of the cases studied around the corresponding centroids of each group.

3. Results

3.1. Qualitative results

Nuclear immunostaining for Snail was observed in the acinar epithelium in all the groups analyzed. Likewise, immunoreactivity for Snail is visualized in the cytoplasm of epithelial cells both in normal cases (CTR) and in pathological cases (BPH and CA). In the CTR and BPH groups, immunoreactivity is detected in both columnar and basal cells. From a qualitative point of view, there are no differences between the cases of the CTR group and the pathological cases of both the BPH and CA groups. Neither do qualitative differences appear to be detected in cytoplasmic immunostaining for Snail in the groups studied (Figure 2a-c). Immunoreactivity to ck 18 was visualized in acini from CTR, BPH, and CA groups (Figure 2d-f).

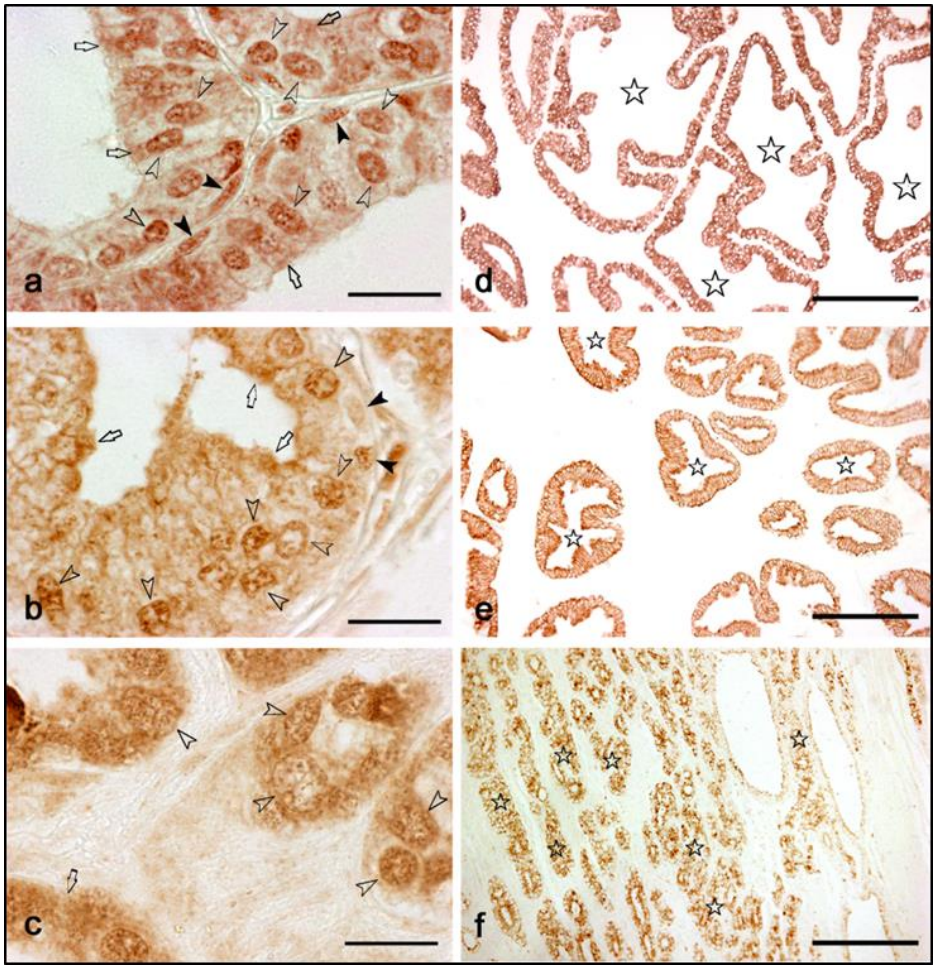

Figure 2 In (a), the image shown is from a case of CTR group, nuclei from both columnar (empty arrowheads) and basal (black arrowheads) cells are immunoreactive to Snail. Immunostaining to Snail was also detected in the cytoplasm (empty arrows). In (b), the image is from a case of the BPH group; nuclei from both columnar (empty arrowheads) and basal (black arrowheads) cells are immunoreactive to Snail. Immunostaining to Snail was abundant in the cytoplasm (empty arrows). In CA group (c) was also detected Snail immunoreactivity in both nuclei (empty arrowheads) and cytoplasms (empty arrows) from acinar tumor cells. Immunoreactivity to ck18 (empty stars) was visualized in acini from CTR (d), BPH (e), and CA (f) groups. The scale bars from (a-c) represent 18 μm, and from (d-f), 180 μm

3.2. Local and global quantitative estimates of Snail and ck18 IOD

When the local estimates of nuclear Snail IOD are compared with the corresponding estimates of cytoplasmic IOD, throughout the spatial series of the data from CTR and BPH groups, it was detected that the cytoplasmic values are significantly higher than the nuclear values in the 46 % of the points of the spatial series of the CTR group and more than 90% of the points of the series of the BPH group (Figure 3 a,b). While in the case of the spatial series of the CA group, no significant differences between nuclear and cytoplasmic IOD are detected at any point (Figure 3c).

When the spatial series of the CTR group are compared with those corresponding to the BPH group, in the case of cytoplasmic Snail IOD, significant differences between both groups are only observed in one location of the series (247 μm from the origin of coordinates). However, the trend is that the highest values correspond to BPH (Figure 4a). For the Snail IOD nuclear series, although the values of the BPH group also tend to be higher than those of the CTR group, there are no significant differences at any point (Figure 4b). No significant differences were observed when comparing the different locations along the spatial series of cytoplasmic Snail IOD in CTR with the corresponding ones in CA (Figure 5a). However, for the spatial series of nuclear Snail IODs, it is detected that in 18% of the locations, the IOD of the CA group is significantly higher than in the CTR group (Figure 5b).

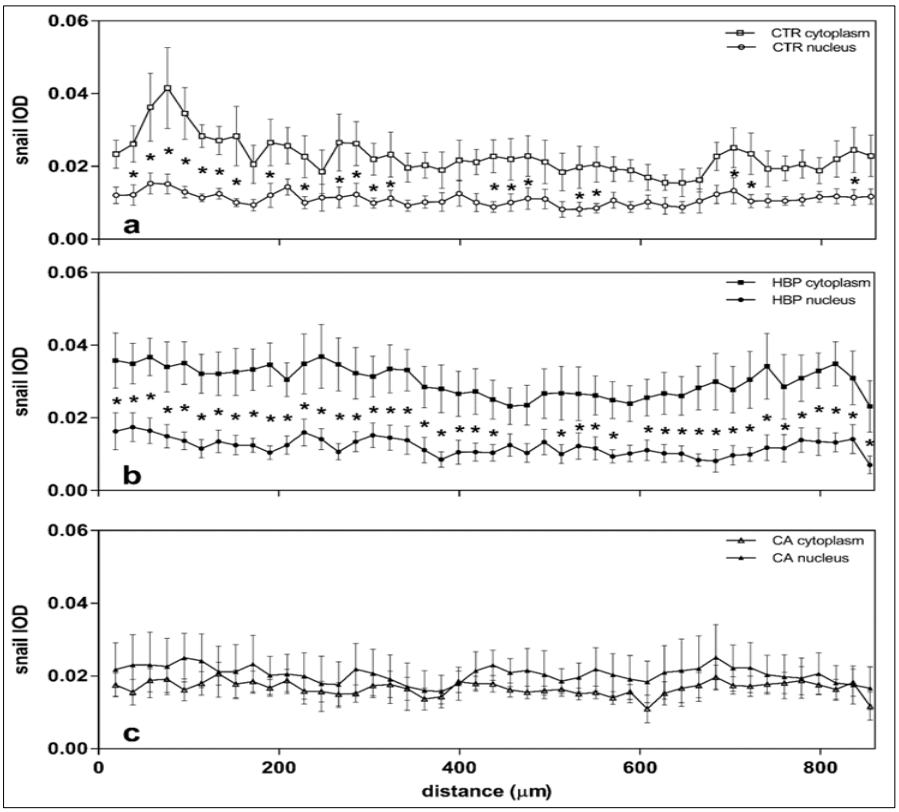

Figure 3 Diagrams for space series of local Snail IOD values along the X-axis (position in μm) of the correspondent strips of CTR cytoplasm versus CTR nucleus (a); HBP cytoplasm versus HBP nucleus (c); CA cytoplasm versus CA nucleus (c). Each point from each diagram represents the mean ± SEM of the values from each space location. The asterisks in (a) and (b) graphs indicate that there are significant differences among the local means affected ($p < 0.05$)

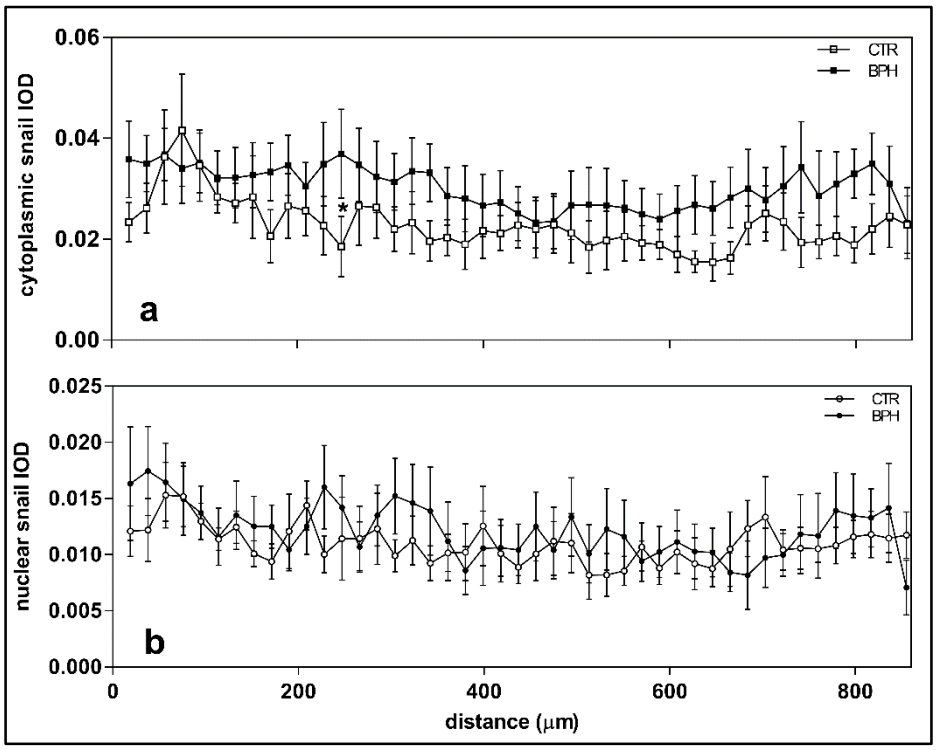

Figure 4 Diagrams for space series of local Snail IOD values along the X-axis (position in μm) of the correspondent strips of CTR cytoplasm versus HBP cytoplasm (a); CTR nucleus versus HBP nucleus (b). Each point from each diagram represents the mean ± SEM of the values from each space location. The asterisk in (a) diagram indicates that there is a significant difference among the local means affected ($p < 0.05$)

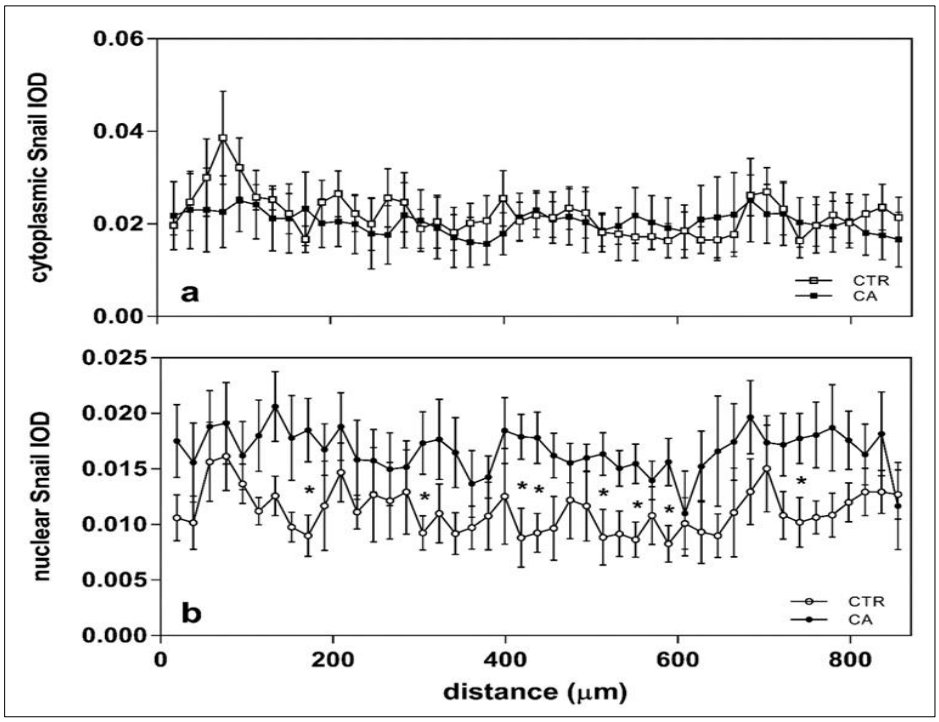

Figure 5 Diagrams for space series of local Snail IOD values along the X-axis (position in μm) of the correspondent strips of CTR cytoplasm versus CA cytoplasm (a); CTR nucleus versus CA nucleus (b). Each point from each diagram represents the mean ± SEM of the values from each space location. The asterisks in the (b) diagram indicate that there are significant differences among the local means affected ($p < 0.05$)

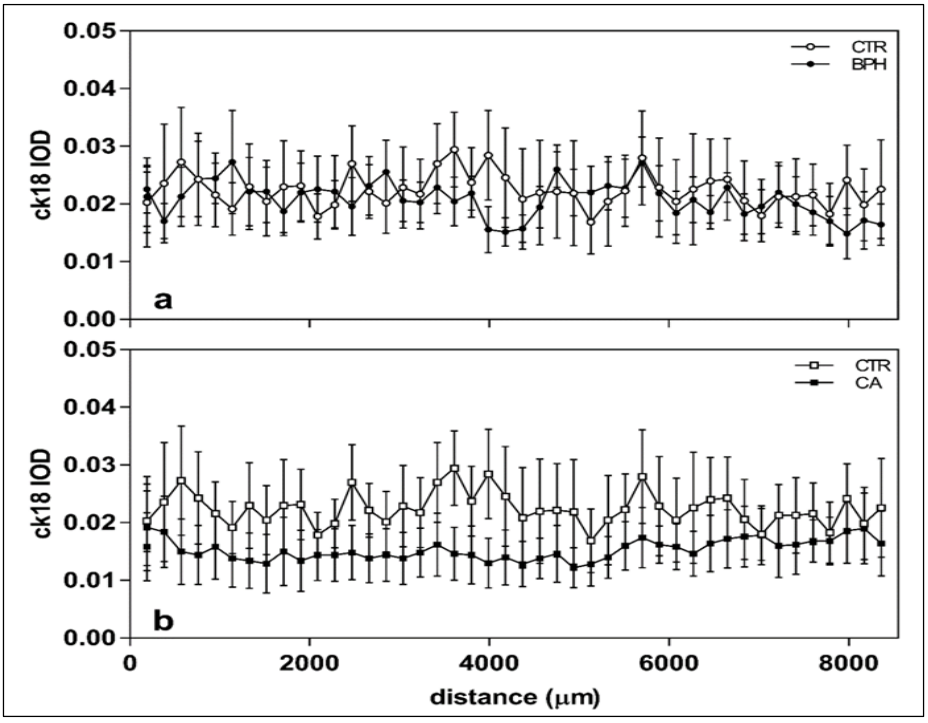

Figure 6 Diagrams for space series of local ck18 values along the X-axis (position in μm) of the correspondent strips of CTR cytoplasm versus BPH cytoplasm (a); CTR cytoplasm versus CA cytoplasm (b). Each point from each diagram represents the mean ± SEM of the values from each space location. None of the local values show significant differences between the space series shown in the diagram ($p < 0.05$)

In the spatial series immunostained for ck18, it is observed that the ck18 IOD in the CTR group does not show significant differences in any location, both when compared with their BPH or CA counterparts. However, it is visualized that the trend in the CA group is that the ck18 IOD is lower throughout the series than in the CTR group (Figure 6a,b).

Globally considered the cytoplasmic and nuclear IOD for Snail immunoreactivity does not show significant differences when comparing the study groups. However, the cytoplasmic IOD seems to be lower in BPH (Figure 7a), while nuclear IOD seems to increase in CA (Figure 7b). As was for the Snail IOD in the global comparison, the global ck18 IOD does not show significant differences between the three study groups, although the values are higher in CTR than in BPH and CA (Figure 7c).

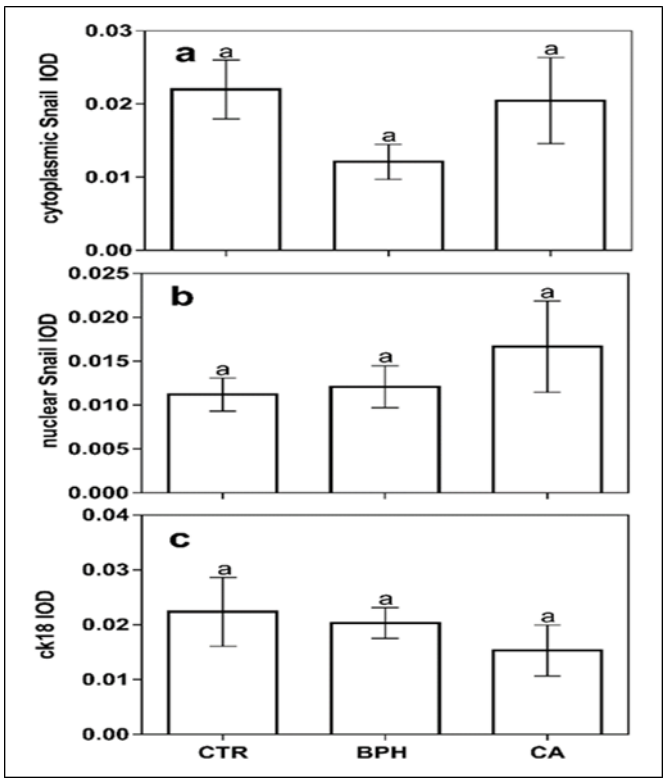

Figure 7 Bar diagrams expressing global mean ± SEM for (a) cytoplasmic Snail IOD, (b) nuclear Snail IOD in CTR, BPH, and CA groups, and (c) for ck18 IOD between CTR, BPH, and CA groups. The letters on the top of error bars indicate the significance. Bars with the same letters do not differ significantly ($p < 0.05$).

3.3. Correlation studies

In CTR and BPH groups, correlation between IOD nuclear Snail and ck18 immunostainings was observed. The linear regression shows a positive slope that was not significantly ≠ 0 ($p = 0.458$) (Figure 8a). However, the IOD values for both cytoplasmic Snail and ck18 immunostainings for the same groups, were adjusted to linear regression with a negative slope that was significantly ≠ 0 ($p < 0.0001$) (Figure 8b). The distribution of points representing the CTR and BPH cases was relatively homogenous along with the graphs, with no trend to clustering (Figure 8a,b).

In CTR and CA groups, in the case of correlation between IOD nuclear Snail and ck18 immunostainings, the linear regression shows a negative slope that was significantly ≠ 0 ($p < 0.0001$) (Figure 8c). However, for the same groups, the IOD values for both cytoplasmic Snail and ck18 immunostainings were adjusted to linear regression with a positive slope that was not significantly ≠ 0 ($p = 0.694$) (Fig. 8d). In the two types of linear regression, the points representing the CA group accumulated in the regions of the graph that show high IOD values for Snail immunostaining and low IOD values for ck18 immunoreactivity (Figure 8c,d).

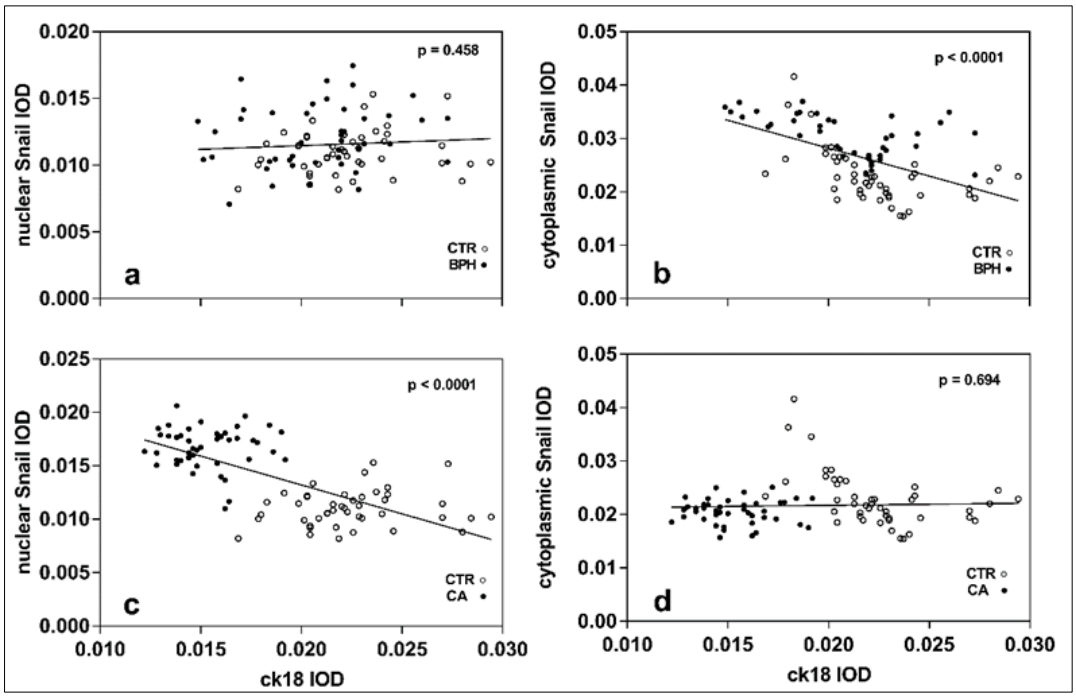

Figure 8 Graphs expressing the linear regression between: CTR and BPH groups for the variables: (a) ck18 IOD and nuclear Snail IOD; (b) ck18 IOD and cytoplasmic Snail IOD; and between CTR and CA groups for the variables: (c) ck18 IOD and nuclear Snail IOD; (d) ck18 IOD and cytoplasmic Snail IOD. The p-values in the upper right corner of each graph indicate the significance of the slope (≠ 0) of the corresponding equation. For images a-d, the cases of the CTR group are represented by empty circles and those of the BPH and CA groups by solid circles

3.4. Discriminant analysis

The discriminant analysis performed to classify the cases in the study groups (CTR, BPH, and CA) reveals that the variables were, ordered for classificatory power:

- Nuclear Snail IOD.
- Cytoplasmic Snail IOD.
- Ck18 IOD.

With these variables in the model, 87% of individuals were correctly classified. Table 1 shows the significant reduction of Wilks' lambda statistic with these variables included in the model.

Table 1 Discriminant analysis to classify the CTR, BPH and CA cases after local IOD variables

Entered variable[1]	Wilks' lambda[2]	F[3]	p[4]
nuclear Snail IOD	0.239	105.901	<0.001
cytoplasmic Snail IOD	0.229	98.972	<0.001
ck18 IOD	0.127	28.217	<0.001

[1]Selected variables. [2]This column shows the Wilks' lambda for every variable entered. [3]F distribution of Snedecor, the F minimum value for entering the variables was 3.84. [4]Level of significance p < 0.05.

The two canonic discriminant functions obtained in the analysis, and represented in a bi-dimensional plot, show an appropriate clustering of points from the individual cases around corresponding group centroids (Figure 9).

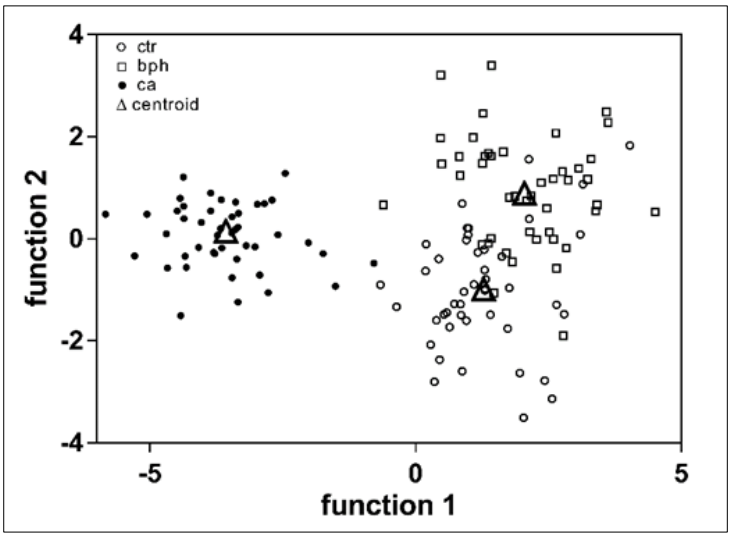

Figure 9 Scatter plot for canonic discriminant functions 1 and 2, obtained after introduction in the analysis of nuclear Snail IOD, cytoplasmic Snail IOD, and ck18 IOD variables. The cases for CTR, BPH, and CA groups are represented by empty circles, empty squares, and solid circles, respectively. The group centroids for CTR, BPH, and CA are depicted by triangles

4. Discussion

It is evident that, both in the normal prostate and in BPH, the immunostaining for Snail estimated by IOD is more relevant at the cytoplasms than at the nuclei, this could be interpreted as in these situations, Snail is mostly in its inactivated (cytoplasmic) form, probably through its ubiquitination [35, 36].

In various tissue locations, it is observed that for the CA group, the IOD of nuclear immunostaining for Snail is significantly higher than for the CTR group. However, overall, no differences are found; this seems to confirm that Snail is expressed locally in prostate cancer, which could have a role in the malignant progression of the tumor as has already been indicated by numerous authors [5, 6]. The fact that the global expression of Snail is not relevant in the cases studied, and its heterogeneity of expression at the local level, would be in agreement with the behavioral variability of prostate cancer in terms of invasiveness and aggressiveness [6, 13, 37].

The IOD of immunostaining for ck18, considered both globally and locally, never showed significant differences between CA, BPH, and CTR; however, the trend observed is that in cancer, the immunoexpression of ck18 is lower in all locations than in BPH and CTR, this may correlate with what has been described in other studies about the lower expression of cytokeratins and other epithelial markers as a consequence of EMT manifested in tumor processes [7, 13].

In a previous study, the local variability of immunoexpression for ck18 in prostate cancer has been verified [38]. In the present work, a correlation was detected between the IOD of immunostaining for Snail with the same parameter for ck18. This correlation was differently manifested according to the groups studied. In the case of BPH plus CTR, it is observed that the increase of IOD for cytoplasmic Snail is significantly associated with a decrease of IOD for ck18; however, this significant association does not occur when the CA and CTR groups are studied together.

When the IOD for nuclear Snail is correlated with the IOD for ck18, the opposite occurs: For BPH plus CTR, it is observed that the increase of IOD for nuclear Snail is not significantly associated with a decrease of IOD for ck18. At the same time, this association is significant when the CA plus CTR groups are studied. These observations confirm what is indicated by other authors [6, 39], that the expression of Snail in the nuclei of tumor cells indicates the activity of this transcription factor related to the down-regulation of epithelial markers such as ck18 [7, 13], while the expression of Snail in the cytoplasm would correspond to inactive Snail [35, 36].

It is interesting to note that when CTR plus BPH are considered together, the cases from the two groups are homogeneously distributed. In contrast, separate clusters from CTR and CA cases are formed when the CTR plus CA are studied. This phenomenon highlights the above mentioned in that in tumor cases the immunoexpression of nuclear Snail is negatively correlated with the immunoreactivity of ck18 as a manifestation of EMT [5, 13].

The discriminant analysis has revealed that the variables that estimate the IOD of immunostaining for Snail (nuclear and cytoplasmic) and the variable that measures the IOD for immunostaining for ck18 have an adequate capacity to

classify the cases into the three groups studied. In other words, the use of these variables allows 87% of cases to indicate whether a specimen is of normal prostate tissue, benign hyperplasia, or cancer. These data emphasize what other authors have highlighted about the pivotal role of Snail repression in developing therapeutic mechanisms leading to inhibition of epithelial to mesenchymal transition in metastatic prostate cancer cells [40, 41].

5. Conclusion

The following conclusions can be drawn from the present study: In all cases, Snail's immunoexpression is heterogeneous with local variations. In prostate cancer, the expression of Snail is abundant at the nuclei. At the same time, in normal and hyperplastic tissue, Snail is mainly cytoplasmic, which may indicate that in these situations, Snail predominates in an inactive form. The expression of Snail is negatively correlated with that of the epithelial marker ck18; this could be correlated with mesenchymal epithelium transition developed in the cancer progression. Snail and ck18 immunoexpression were able to discriminate between normal, hyperplastic, and malignant prostate tissues.

Compliance with ethical standards

Acknowledgments

The authors would like to thank for technical support to Carmen Sanchez (Department of Anatomy, Histology, and Neuroscience, UAM).

Disclosure of conflict of interest

No conflict of interest.

Statement of ethical approval

The present research work does not contain any studies with human participants or animals performed by any of the authors.

Statement of informed consent

Informed consent for the use of surgical specimens or biopsies, issued by the Bioethics Committee of the Hospital Universitario de La Princesa (Madrid, Spain) was accomplished to obtain the prostate tissue either when the multi-organic extraction for transplant (CTR) or at the surgery (CA).

References

[1] Santamaria L, Ingelmo I, Teba F, Coloma A, Martínez L. Quantitative stereological estimations of structural patterns of the glandular tree in benign hyperplasia of prostate. Open Journal of Pathology 2016;6(3):122-33. https://doi.org/10.4236/ojpathology.2016.63015

[2] Park Y, Lim S, Nam JW, Kim S. Measuring intratumor heterogeneity by network entropy using RNA-seq data. Sci Rep. 2016;6:37767. https://doi.org/10.1038/srep37767

[3] Santamaria L, Ingelmo Ingelmo I, Rodriguez Ramos R, Sinues Ojas B, Martinez Blazquez L, Teba del Pino F. Estimate of the K function and isotropy of acini in human normal prostate and prostate adenocarcinoma. Histol Histopathol. 2015;30(Suppl 1):149-50.

[4] Lindsay CR, Le Moulec S, Billiot F, Loriot Y, Ngo-Camus M, Vielh P, Fizazi K, Massard C, Farace F. Vimentin and Ki67 expression in circulating tumour cells derived from castrate-resistant prostate cancer. BMC Cancer. 2016;16:168. https://doi.org/10.1186/s12885-016-2192-6

[5] Odero-Marah V, Hawsawi O, Henderson V, Sweeney J. Epithelial-Mesenchymal Transition (EMT) and Prostate Cancer. Adv Exp Med Biol. 2018;1095:101-10. https://doi.org/10.1007/978-3-319-95693-0_6

[6] Burton LJ, Hawsawi O, Loyd Q, Henderson V, Howard S, Harlemon M, Ragin C, Roberts R, Bowen N, Gacii A, Odero-Marah V. Association of Epithelial Mesenchymal Transition with prostate and breast health disparities. PLoS One. 2018;13(9):e0203855. https://doi.org/10.1371/journal.pone.0203855

[7] Grant CM and Kyprianou N. Epithelial mesenchymal transition (EMT) in prostate growth and tumor progression. Transl Androl Urol. 2013;2(3):202-11. https://doi.org/10.3978/j.issn.2223-4683.2013.09.04

[8] Kalluri R and Weinberg RA. The basics of epithelial-mesenchymal transition. J Clin Invest. 2009;119(6):1420-8. https://doi.org/10.1172/JCI39104

[9] Alonso-Magdalena P, Brossner C, Reiner A, Cheng G, Sugiyama N, Warner M, Gustafsson JA. A role for epithelial-mesenchymal transition in the etiology of benign prostatic hyperplasia. Proc Natl Acad Sci U S A. 2009;106(8):2859-63. https://doi.org/10.1073/pnas.0812666106

[10] Wallerand H, Robert G, Pasticier G, Ravaud A, Ballanger P, Reiter RE, Ferriere JM. The epithelial-mesenchymal transition-inducing factor TWIST is an attractive target in advanced and/or metastatic bladder and prostate cancers. Urol Oncol. 2010;28(5):473-9. https://doi.org/10.1016/j.urolonc.2008.12.018

[11] Zhou BP, Deng J, Xia W, Xu J, Li YM, Gunduz M, Hung MC. Dual regulation of Snail by GSK-3beta-mediated phosphorylation in control of epithelial-mesenchymal transition. Nat Cell Biol. 2004;6(10):931-40. https://doi.org/10.1038/ncb1173

[12] Grau Y, Carteret C, Simpson P. Mutations and Chromosomal Rearrangements Affecting the Expression of Snail, a Gene Involved in Embryonic Patterning in Drosophila Melanogaster. Genetics. 1984;108(2):347-60. https://doi.org/10.1093/genetics/108.2.347

[13] Nieto MA. The snail superfamily of zinc-finger transcription factors. Nat Rev Mol Cell Biol. 2002;3(3):155-66. https://doi.org/10.1038/nrm757

[14] Nüsslein-Volhard C, Wieschaus E, Kluding H. Mutations affecting the pattern of the larval cuticle inDrosophila melanogaster : I. Zygotic loci on the second chromosome. Wilehm Roux Arch Dev Biol. 1984;193(5):267-82. https://doi.org/10.1007/BF00848156

[15] Alberga A, Boulay JL, Kempe E, Dennefeld C, Haenlin M. The snail gene required for mesoderm formation in Drosophila is expressed dynamically in derivatives of all three germ layers. Development. 1991;111(4):983-92.

[16] Batlle E, Sancho E, Franci C, Dominguez D, Monfar M, Baulida J, Garcia De Herreros A. The transcription factor snail is a repressor of E-cadherin gene expression in epithelial tumour cells. Nat Cell Biol. 2000;2(2):84-9. https://doi.org/10.1038/35000034

[17] Cano A, Perez-Moreno MA, Rodrigo I, Locascio A, Blanco MJ, del Barrio MG, Portillo F, Nieto MA. The transcription factor snail controls epithelial-mesenchymal transitions by repressing E-cadherin expression. Nat Cell Biol. 2000;2(2):76-83. https://doi.org/10.1038/35000025

[18] Epstein JI, Allsbrook WC, Jr., Amin MB, Egevad LL, Committee IG. The 2005 International Society of Urological Pathology (ISUP) Consensus Conference on Gleason Grading of Prostatic Carcinoma. The American Journal of Surgical Pathology. 2005;29(9):1228-42. https://doi.org/10.1097/01.pas.0000173646.99337.b1

[19] Egevad L, Mazzucchelli R, Montironi R. Implications of the International Society of Urological Pathology modified Gleason grading system. Archives of pathology and laboratory medicine. 2012;136(4):426-34. https://doi.org/10.5858/arpa.2011-0495-RA

[20] Howard CV and Reed MG. Unbiased Stereology: three-dimensional measurement in microscopy. Oxford. Bios Scientific Publishers. 2005.

[21] Martin JJ, Martin R, Codesal J, Fraile B, Paniagua R, Santamaria L. Cadmium chloride-induced dysplastic changes in the ventral rat prostate: an immunohistochemical and quantitative study. Prostate. 2001;46(1):11-20. https://doi.org/10.1002/1097-0045(200101)46:1<11::aid-pros1003>3.0.co;2-k

[22] Gomez V, Ingelmo I, Martin R, Codesal J, Rodriguez R, Pozuelo JM, Santamaria L. Effect of prolactin on the population of epithelial cells from ventral prostate of intact and cyproterone acetate-treated peripubertal rats: stereological and immunohistochemical study. Anatomical record (Hoboken). 2009;292(5):746-55. https://doi.org/10.1002/ar.20879

[23] Santamaria L, Andres Delgado L, Chaves I, Ingelmo I, Teba F. Stereological estimates of length and surface densities of the acini from normal and pathological prostate: global and local differences. Histol Histopathol. 2017;32(Suppl 1):98.

[24] Santamaria L, Ingelmo I, Ruiz J, Teba F, Herranz LM, Montalban G, Martin R, Codesal J, Pozuelo JM, Rodriguez R, Arriazu R. Stereological Estimate of the Length of Microvessels and the Number, Proliferation and Apoptosis of Endothelial Cells in Prostate Cancer. The Open Prostate Cancer Journal. 2009;2:46-53. https://doi.org/10.2174/1876822900902010046

[25] Gundersen HJ and Osterby R. Optimizing sampling efficiency of stereological studies in biology: or ‘‘do more less well!’’. J Microsc. 1981;121(Pt 1):65-73. https://doi.org/10.1111/j.1365-2818.1981.tb01199.x.

[26] Santamaria L, Ingelmo I, Ruiz J, Teba F. Study of the distribution of microvessels in normal and pathologic prostate using an information-based similarity analysis. J Microsc. 2011;243(3):303-14. https://doi.org/10.1111/j.1365-2818.2011.03508.x

[27] Rasband WS and Bright DS. NIH Image: A Public Domain Image Processing Program for the Macintosh. Microbeam Analysis Soc Jour. 1995;4:137-49.

[28] Huang Y, Zhu L, Tan J, Guo W, Yang Z, Shi W, Yu B. Correlation between SHP-1 and carotid plaque vulnerability in humans. Cardiovasc Pathol. 2020;49:107258. https://doi.org/10.1016/j.carpath.2020.107258

[29] Xu F, Ren ZX, Zhong XM, Zhang Q, Zhang JY, Yang J. Intrauterine Inflammation Damages Placental Angiogenesis via Wnt5a-Flt1 Activation. Inflammation. 2019;42(3):818-25. https://doi.org/10.1007/s10753-018-0936-y

[30] Wicht H, Maronde E, Olcese J, Korf HW. A semiquantitative image-analytical method for the recording of dose-response curves in immunocytochemical preparations. J Histochem Cytochem. 1999;47(3):411-20. https://doi.org/10.1177/002215549904700315

[31] Singh G, Sankanagoudar S, Dogra P, Chandra NC. Interlink between cholesterol & cell cycle in prostate carcinoma. Indian J Med Res. 2017;146(Suppl):S38-S44. https://doi.org/10.4103/ijmr.IJMR_1639_15

[32] Zhang M, Ho A, Hammond EH, Suzuki Y, Bermudez RS, Lee RJ, Pilepich M, Shipley WU, Sandler H, Khor LY, Pollack A, Chakravarti A. Prognostic value of survivin in locally advanced prostate cancer: study based on RTOG 8610. Int J Radiat Oncol Biol Phys. 2009;73(4):1033-42. https://doi.org/10.1016/j.ijrobp.2008.06.1489

[33] Tilley WD, Lim-Tio SS, Horsfall DJ, Aspinall JO, Marshall VR, Skinner JM. Detection of discrete androgen receptor epitopes in prostate cancer by immunostaining: measurement by color video image analysis. Cancer Res. 1994;54(15):4096-102.

[34] Hair J, Anderson RE, Tatham RL, Black WC. Multivariate Data Analysis. New Jersey. Prentice Hall. 1998.

[35] Ko H, Kim HS, Kim NH, Lee SH, Kim KH, Hong SH, Yook JI. Nuclear localization signals of the E-cadherin transcriptional repressor Snail. Cells Tissues Organs. 2007;185(1-3):66-72. https://doi.org/10.1159/000101305

[36] Sinha N, Meher BR, Naik PP, Panda PK, Mukhapadhyay S, Maiti TK, Bhutia SK. p73 induction by Abrus agglutinin facilitates Snail ubiquitination to inhibit epithelial to mesenchymal transition in oral cancer. Phytomedicine. 2019;55:179-90. https://doi.org/10.1016/j.phymed.2018.08.003

[37] Lamouille S, Xu J, Derynck R. Molecular mechanisms of epithelial-mesenchymal transition. Nat Rev Mol Cell Biol. 2014;15(3):178-96. https://doi.org/10.1038/nrm3758

[38] Santamaria L, Ingelmo I, Sinues B, Martinez L, Teba F. Quantification of the heterogeneity of cytokeratin 18 immunoexpression in prostate adenocarcinoma and normal prostate: Global and local features. Histol Histopathol. 2018;33(10):1099-110. https://doi.org/10.14670/HH-18-009

[39] Rosivatz E, Becker KF, Kremmer E, Schott C, Blechschmidt K, Hofler H, Sarbia M. Expression and nuclear localization of Snail, an E-cadherin repressor, in adenocarcinomas of the upper gastrointestinal tract. Virchows Arch. 2006;448(3):277-87. https://doi.org/10.1007/s00428-005-0118-9

[40] Bonavida B and Baritaki S. Dual role of NO donors in the reversal of tumor cell resistance and EMT: Downregulation of the NF-kappaB/Snail/YY1/RKIP circuitry. Nitric Oxide. 2011;24(1):1-7. https://doi.org/10.1016/j.niox.2010.10.001

[41] Oh BS, Im E, Lee HJ, Sim DY, Park JE, Park WY, Park Y, Koo J, Pak JN, Kim DH, Shim BS, Kim SH. Inhibition of TMPRSS4 mediated epithelial-mesenchymal transition is critically involved in antimetastatic effect of melatonin in colorectal cancers. Phytother Res. 2021;35(8):4538-46. https://doi.org/10.1002/ptr.7156